# Dynamic Pile Response During Vibratory Driving and Modal-Based Strain Field Mapping

Gómez, Sergio S.; Tsetas, Athanasios; Tsouvalas, Apostolos; Metrikine, Andrei V.

**DOI**
10.1007/978-3-031-15758-5_116

**Publication date**
2023

**Document Version**
Final published version

**Published in**
Recent Trends in Wave Mechanics and Vibrations - Proceedings of WMVC 2022

**Citation (APA)**
Gómez, S. S., Tsetas, A., Tsouvalas, A., & Metrikine, A. V. (2023). Dynamic Pile Response During Vibratory Driving and Modal-Based Strain Field Mapping. In Z. Dimitrovová, R. Gonçalves, Z. Dimitrovová, P. Biswas, & T. Silva (Eds.), *Recent Trends in Wave Mechanics and Vibrations - Proceedings of WMVC 2022* (pp. 1125-1134). (Mechanisms and Machine Science; Vol. 125 MMS). Springer. https://doi.org/10.1007/978-3-031-15758-5_116

**Important note**
To cite this publication, please use the final published version (if applicable).
Please check the document version above.

# Dynamic Pile Response During Vibratory Driving and Modal-Based Strain Field Mapping

Sergio S. Gómez(✉), Athanasios Tsetas, Apostolos Tsouvalas, and Andrei V. Metrikine

Faculty of Civil Engineering and Geosciences, Delft University of Technology, Stevinweg 1, 2628 CN Delft, The Netherlands
{s.sanchezgomez-1,a.tsetas,a.tsouvalas,a.metrikine}@tudelft.nl

**Abstract.** For offshore wind turbines (OWTs), the monopile comprises the most common type of foundation and vibratory driving is one of the main techniques for monopile installation (and decommissioning). In practice, prior to pile installation, a pile driving analysis is performed to select the appropriate installation device and the relevant settings. However, pile penetration results from a complicated vibrator-pile-soil interaction and better understanding of the latter is necessary for an efficient installation process. During the course of installation, the interface and boundary conditions of the pile continuously alter due to the soil layering and the non-linearity of the soil reaction. In this paper, a set of experimental data from an onshore experimental campaign are employed in a numerical scheme to identify the pile strain field based on *in vacuo* modes of simpler yet related systems. By mapping the pile strain field onto physically-based shape functions, the evolution of the soil reaction during pile installation can be studied, in order to facilitate the back-analysis of driving records and, by extension, improve pile drivability and vibro-acoustics predictions.

**Keywords:** Pile driving · Vibrations of shells · Mode-matching · Soil-structure interaction

## 1 Introduction

The installation of monopile foundations for offshore wind turbines (OWTs) is one of the most critical phases during the construction of an offshore wind farm [6]. Customarily, the monopile installation is performed via impact hammering, albeit this method has raised significant environmental concerns in the past decade due to underwater noise emissions [5]. In response to these concerns, alternative installation methods are examined with vibratory pile driving being one of the most suitable candidates. This method poses a number of open


Z. Dimitrovová et al. (Eds.): WMVC 2022, MMS 125, pp. 1125–1134, 2023.
https://doi.org/10.1007/978-3-031-15758-5_116

research questions stemming from the complex vibrator-pile-soil interaction during installation. To that end, inflow of new field data and development of suitable numerical approaches for analysis and prediction purposes are necessary to improve our understanding of vibratory pile driving.

In line with this work, an experimental campaign has been performed, which included installation tests via different driving methods, i.e. axial vibratory driving (VH) and the novel 'Gentle Driving of Piles' (GDP) [3,4]. The latter method introduces a high-frequency torsional excitation in addition to the classical axial vibration to improve the installation performance and reduce noise emissions. The collected data of the instrumented piles that were installed by means of the already mentioned pile driving techniques are used.

In this paper, a set of experimental data from the GDP campaign are employed to study the pile response during installation. The pile is modelled as a thin cylindrical shell and the modes *in vacuo* are found for two limit case configurations, i.e. for both ends being i) free and ii) fixed. These two modal sets are combined and the recorded axial strain is mapped onto them, as they can address stresses at the pile ends, as well as admit rigid body motion which is essential for pile penetration. The mode-matching process is performed by means of a least-squares optimization and the obtained field is in great agreement with the field measurements. Conclusively, this approach can be valuable for back-analysis of field measurements and aid in the identification of the dynamic soil reaction during driving, which is one of the most uncertain parameters in vibratory pile installation.

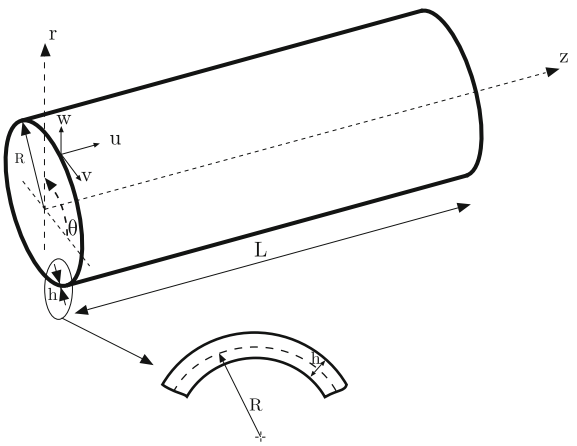


**Fig. 1.** Geometry and coordinate system of a cylindrical shell.

## 2 Governing Equations

A linear elastic cylindrical shell is considered, with finite length $L$, radius $R$, and wall thickness $h$, as shown in Fig. 1.The equations of motion of a cylindrical shell can be written in the following general form:

$$(\mathbf{L} + \mathbf{I})\,\mathbf{u} = \mathbf{0} \tag{1}$$

where $\mathbf{L}$ and $\mathbf{I}$ are the stiffness and inertial operators, respectively. The vector $\mathbf{u} = \begin{bmatrix} u\ v\ w \end{bmatrix}^{\mathrm{T}}$ describes the displacement of the mid-surface of the shell in the cylindrical coordinate system $(r, \theta, z)$. In this work, the shell motion is considered axisymmetric (i.e. $\partial(\cdot)/\partial\theta = 0$) and the membrane shell theory is employed to describe the pile [1]. Therefore, the non-zero elements $L_{ij}$ and $I_{ij}$ of the stiffness and inertial operators are defined as [2]:

$$\begin{gathered} L_{11} = \frac{\partial^2}{\partial z^2},\ L_{13} = \frac{\nu}{R}\frac{\partial}{\partial z},\ L_{22} = \frac{1-\nu}{2}\frac{\partial^2}{\partial z^2},\ L_{31} - \frac{\nu}{R}\frac{\partial}{\partial z},\ L_{33} = -\frac{1}{R^2}, \\ I_{11} = I_{22} = I_{33} = -\frac{1}{c^2}\frac{\partial^2}{\partial t^2} \end{gathered} \tag{2}$$

where $c = \sqrt{E/\left(\rho(1-\nu^2)\right)}$ is the thin plate wave velocity, $E$ is the Young's modulus, $\rho$ is the mass density and $\nu$ is the Poisson ratio of the shell material. From Eq. (2), it can be noted that the circumferential motion $(v)$ is uncoupled from the longitudinal $(u)$ and radial $(w)$ motions of the shell, due to the axisymmetric conditions. For the coupled axial-radial motion of the shell, the solution to the axisymmetric free vibration problem reads:

$$\begin{aligned} u(z,t) &= \sum_{i=1}^{\infty} U_i(z) q_i(t) \\ w(z,t) &= \sum_{i=1}^{\infty} W_i(z) q_i(t) \end{aligned} \tag{3}$$

where $U_i(z)$ and $W_i(z)$ are the axial and radial modal displacements of the $i$-th mode, respectively, and $q_i(t)$ is the corresponding modal coordinate. For the case of a shell that is clamped at both ends, the boundary conditions read:

$$u(z=0,t) = u(z=L,t) = 0 \tag{4}$$

while in the case of a shell with traction-free ends, the boundary conditions read:

$$N_{zz}(z=0,t) = N_{zz}(z=L,t) = 0 \tag{5}$$

where $N_{zz}$ is the so-called axial force resultant. By substitution of Eq. (3) into Eq. (1), the free vibration problem can be formulated and the axial wavenumbers and

natural frequencies of the cylindrical shell can be found. The relevant treatment is well-known in the topic of shell vibrations [2] and will be omitted here for brevity. The free vibration solutions are given for the case of clamped-clamped (C-C):

$$\begin{aligned} u_{\mathrm{c}}(z,t) &= \sum_{i=1}^{\infty} \sin(\gamma_i z) q_i(t) \\ w_{\mathrm{c}}(z,t) &= \sum_{i=1}^{\infty} \frac{\nu R \gamma_i c^2}{R^2\omega_i^2 - c^2} \cos(\gamma_i z) q_i(t) \end{aligned} \tag{6}$$

and free-free (F-F) boundary conditions:

$$\begin{aligned} u_{\mathrm{f}}(z,t) &= \sum_{i=0}^{\infty} \cos(\gamma_i z) q_i(t) \\ w_{\mathrm{f}}(z,t) &= \sum_{i=0}^{\infty} \frac{-\nu R \gamma_i c^2}{R^2\omega_i^2 - c^2} \sin(\gamma_i z) q_i(t) \end{aligned} \tag{7}$$

where $\omega_i$ and $\gamma_i = \omega_i \sqrt{\left(R^2\omega_i^2 - c^2\right) / \left(c^2(R^2\omega_i^2 - c^2(1-\nu^2))\right)}$ denote the $i$-th natural frequency and the $i$-th axial wavenumber of the cylindrical shell. As can be seen, the index of the F-F shell modes begins from $i = 0$, which corresponds to the rigid body mode of axial translation. The two chosen configurations will be used in Sect. 5 in an optimization scheme for the analysis of the experimental data, as they correspond to two limit cases of the pile during installation.

## 3 Experimental Tests

The experimental data presented and analysed in this paper were obtained during the GDP field tests campaign executed at the Maaskvlakte II in the Port of Rotterdam (the Netherlands) [3,4]. During the GDP tests, a number of piles were installed by means of different driving methods. The present work focuses on two different driving methods, namely the axial vibratory driving (VH) and the GDP method. The geometrical characteristics of the test piles are described in Table 1.

As regards to the pile instrumentation, the types and locations of the pile sensors are shown in Fig. 2. It is remarked that two vertical series of sensors were installed at diametrically opposite locations along the pile circumference (i.e. $\theta = 0$ and $\theta = \pi$). The sampling frequency was set equal to 1 kHz for all sensors.

The same installation protocol was followed for all tested piles. Specifically, in the first 3 m of penetration, the pile was laterally supported to eliminate any inclination that may develop during installation in shallow depth. Therefore, all the results presented in this paper correspond to final 5 m of pile penetration (from 3 m to 8 m), in which the pile was unrestrained and penetrated into the soil under the shaker excitation and its self-weight.

**Table 1.** Geometrical characteristics of the piles.

| Length | Embedded length | Outer diameter | Thickness |
|---|---|---|---|
| $L$ | $L_e$ | $D_o$ | $h$ |
| 10 m | 8 m | 0.762 m | 0.0159 mm |

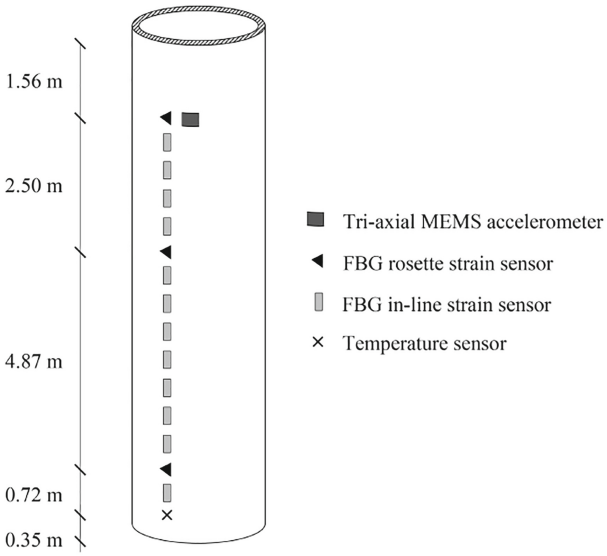


**Fig. 2.** Instrumentation of test piles.

## 4 Mapping of the Strain Field Based on Mode-Matching

In order to gain insight into the structural response of the pile during installation, the axial strains ($\varepsilon_{zz}$) along the pile length are studied. Furthermore, a process to map the recorded strains onto appropriate shape functions for post-processing purposes is presented. Specifically, the free vibration modes *in vacuo* of the cylindrical shell (see Sect. 2) are employed in this process. The two shell configurations, outlined in Sect. 2 (i.e. C-C and F-F), comprise two limit cases for the pile during installation, as both of its ends have tractions (C-C case) and rigid body motion is admissible (F-F case). Therefore, an optimization process is set up to obtain the multipliers of each mode from the C-C and F-F sets, such that the axial strain data and the mode-matching based strains agree during the whole installation process. The strain error $R_\varepsilon(z_j, t_k)$ at each sensor location $z_j$ and time moment $t_k$ is used in a least-squares optimization process to obtain the $q_i(t_k)$:

$$R_\varepsilon(z_j,t_k)=\hat{\varepsilon}_{zz}(z_j,t_k)-\varepsilon_{zz}(z_j,t_k)=\frac{\partial\hat{u}(z_j,t_k)}{\partial z}-\sum_{i=1}^{N}\frac{\partial U_i(z_j)}{\partial z}q_i(t_k) \tag{8}$$

where $\hat{\varepsilon}_{zz}(z_j,t_k)$ and $\varepsilon_{zz}(z_j,t_k)$ denote the measured and computed axial strain, respectively. By $N$ the total amount of modes from both C-C and F-F sets is denoted and accordingly these functions are arranged in the following matrix form:

$$\mathbf{U}_\mathrm{m}=\begin{bmatrix}\mathbf{U}_\mathrm{c}\ \mathbf{U}_\mathrm{f}\end{bmatrix}=\begin{bmatrix}U_{\mathrm{c},1}(z_1) & \dots & U_{\mathrm{c},N_\mathrm{c}}(z_1) & U_{\mathrm{f},0}(z_1) & \dots & U_{\mathrm{f},N_\mathrm{f}-1}(z_1)\\ \vdots & \ddots & \vdots & \vdots & \ddots & \\ U_{\mathrm{c},1}(z_M) & \dots & U_{\mathrm{c},N_\mathrm{c}}(z_M) & U_{\mathrm{f},0}(z_M) & \dots & U_{\mathrm{f},N_\mathrm{f}-1}(z_M)\end{bmatrix} \tag{9}$$

where the matrices $\mathbf{U}_\mathrm{c}$ and $\mathbf{U}_\mathrm{f}$ encapsulate the C-C and F-F modal sets at the sensor location points $z_j$. The respective number of modes included from each set (i.e. $N_\mathrm{c}$ and $N_\mathrm{f}$) can vary such that greater agreement between the measured data and the model computation can be acquired.

The data collected by the diametrically opposite FBG sensors (at the same height level) are averaged and the offset is removed via high-pass filtering. Given the total amount of averaged signals ($M=12$), we adopt the following constraint in the mode-matching optimization process: $N_\mathrm{c}+N_\mathrm{f}\leq M$, such that the number of unknowns $q_i(t_k)$ does not exceed the number of equations at hand.

## 5 Results

In this section, the structural response of two piles installed by means of two distinct pile driving techniques (i.e. VH and GDP) is presented. First, in Fig. 3 the time-frequency analysis of the longitudinal acceleration ($\partial^2u/\partial t^2$) of the two piles during installation is shown in the form of a spectrogram. As can be seen, the axial driving frequency was approximately 16 Hz for the GDP pile and 25 Hz for the VH pile. In the spectrograms of both piles, super-harmonics of the driving frequency with appreciable magnitude are present. In principle, the driving process can be considered almost stationary as the frequency components and their respective magnitudes are approximately constant during the pile installation.

In Fig. 3, information of the frequency content of the pile motion and its temporal evolution can be extracted. As regards to the spatial distribution of the pile deformation, the axial strains (see Fig. 2) along the pile length are employed. The mode-matching process presented in Sect. 4 is applied to the axial strain data and the results are shown in Figs. 4 and 5. For the problem at hand, $N_\mathrm{c}=N_\mathrm{f}=6$ is chosen in the analysis.

The results of the optimization process shown in Fig. 4 indicate that the mode-matching based fit is in great agreement with the experimental data for three distinct penetration depths(4 m, 6 m and 8 m). As can be seen, the strains

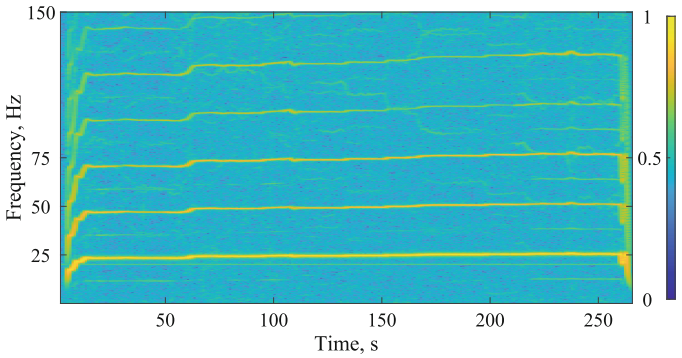


(a) VH Pile

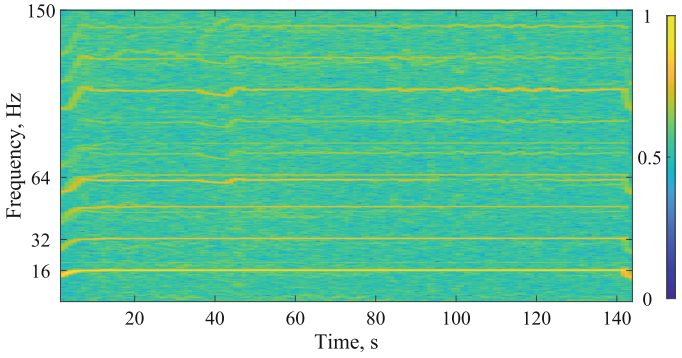


(b) GDP pile

**Fig. 3.** Normalized time-frequency spectrum of the pile acceleration in the longitudinal direction ($\partial^2 u/\partial t^2$) for (a) the VH pile and (b) the GDP pile.

are relatively uniform along the pile for any time moment, with decreasing amplitude from the top to the pile tip resulting from the soil reaction at the pile shaft.

In the case of pile GDP, the mode-matching results appear to be in agreement with the data as well (see Fig. 5). The spatial distribution of the axial strains slightly deviated from the respective patterns observed in the case of the VH pile. By comparing Fig. 3(a) and 3(b), one can note that the number of frequency components with appreciable amplitude are many more in the case of the GDP pile. This is a result of the potential interaction between the axial and torsional motion and results in the richer vibration pattern observed compared to the VH pile, albeit the main trend of diminishing axial strain amplitude with depth is present in both piles.

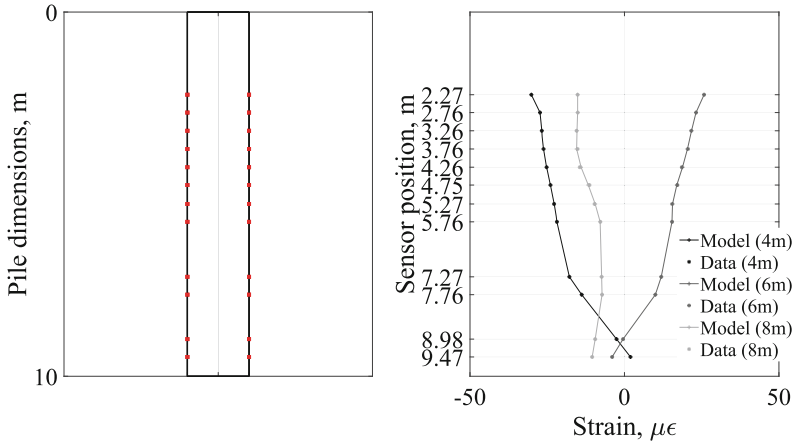


**Fig. 4.** Mode-matching based fit of the axial strain data of the VH pile at three different penetration depths (4 m, 6 m and 8 m).

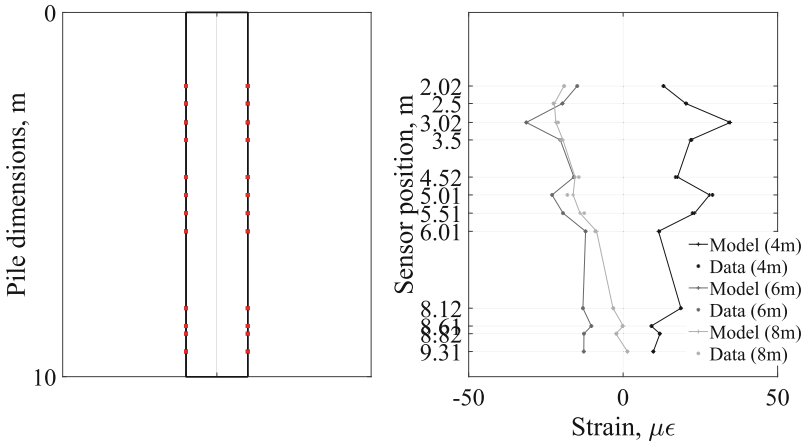


**Fig. 5.** Mode-matching based fit of the axial strain data of the GDP pile at three different penetration depths (4 m, 6 m and 8 m).

In Figs. 6 and 7 the axial strain shapes at different time moments are presented, during one period of vibration and around 6 m of penetration depth. The axial strain shown in Figs. 6 and 7 corresponds to the sensor at the top of the pile in both cases. The observations from Figs. 4 and 5 are further supported, and the response of the GDP pile also resembles the periodic pattern seen in the VH pile.

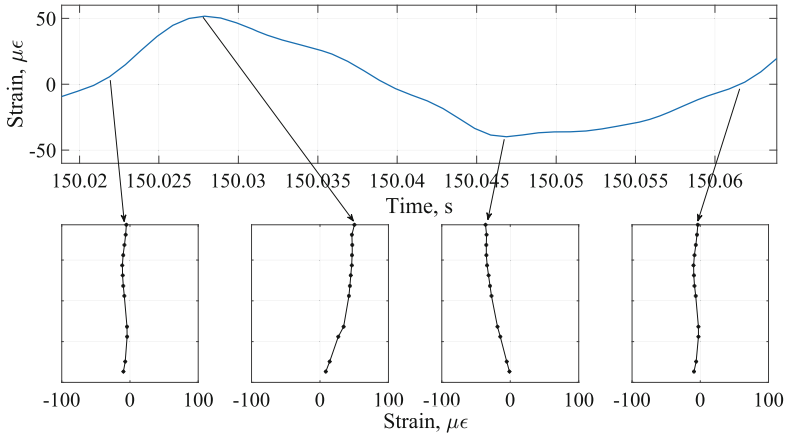


**Fig. 6.** Spatial distribution of axial strains for the VH pile at different time moments around 6 m penetration depth.

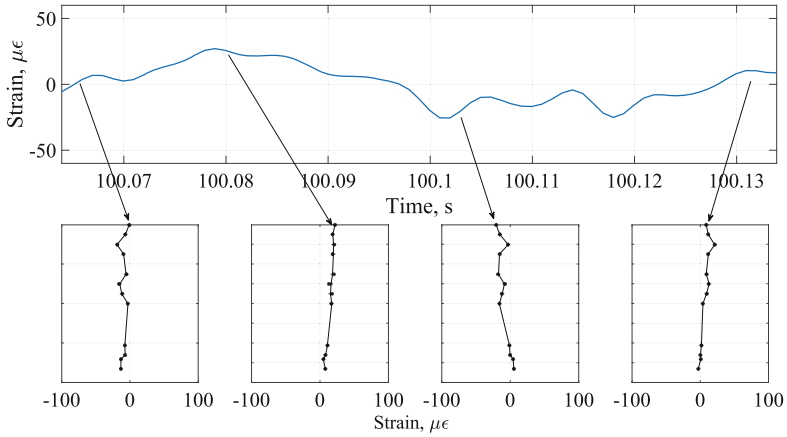


**Fig. 7.** Spatial distribution of axial strains for the GDP pile at different time moments around 6 m penetration depth.

## 6 Conclusions

In this paper, a set of field data from the GDP field campaign are analysed with a focus on the pile structural response during installation. The pile vibrations indicate that the vibratory driving is an almost stationary process, as the frequency components and their respective magnitudes are approximately constant during the pile installation. Furthermore, a mode-matching procedure is developed and applied to two test piles, with a view to map the strain field onto two distinct sets of *in vacuo* pile modes. The mode-matching derived strain field is in great agreement with the strain field data for all the cases examined.

The proposed mode-matching approach is considered to be a valuable tool for analysing and processing such datasets in the absence of extensive/dense instrumentation. The utilization of the present approach can aid in both research and engineering practice works such as the identification of the dynamic soil reaction during installation, the back-analysis of penetration records and the source identification/description for vibro-acoustics modelling.

**Acknowledgments.** This research is associated with the GDP project in the framework of the GROW joint research program. Funding from "Top sector Energie subsidie van het Ministerie van Econsomische Zaken" under grant number TE-HE117100 and financial/technical support from the following partners is gratefully acknowledged: Royal Boskalis Westminster N.V., CAPE Holland B.V., Deltares, Delft Offshore Turbine B.V., Delft University of Technology, ECN, Eneco Wind B.V., IHC IQIP B.V., RWE Offshore Wind Netherlands B.V., SHL Offshore Contractors B.V., Shell Global Solutions International B.V., Sif Netherlands B.V., TNO and Van Oord Offshore Wind Projects B.V.

## References

1. Graff, K.: Wave Motion in Elastic Solids. Oxford University Press (1975)
2. Leissa, A.W.: Vibration of shells, vol. 288. Scientific and Technical Information Office, National Aeronautics and Space Administration (1973)
3. Metrikine, A.V., et al.: GDP: a new technology for gentle driving of (mono)piles. In: Proceedings of the 4th International Symposium on Frontiers in Offshore Geotechnics, Austin, TX, USA, 16–19 August 2020 (2020)
4. Tsetas, A., et al.: Experimental identification of the dynamic behaviour of pile-soil system installed by means of three different pile-driving techniques. In: Proceedings of the XI International Conference on Structural Dynamics, EURODYN 2020. vol. II, pp. 3005–3015. European Association for Structural Dynamics (2020)
5. Tsouvalas, A.: Underwater noise emission due to offshore pile installation: a review. Energies **13**(12), 3037 (2020)
6. Wu, X., et al.: Foundations of offshore wind turbines: a review. Renew. Sustain. Energy Rev. **104**, 379–393 (2019)